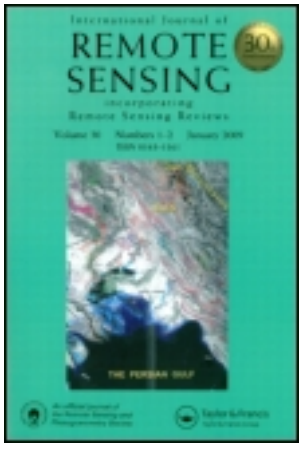

International Journal of Remote Sensing

Publication details, including instructions for authors and subscription information:
http://www.tandfonline.com/loi/tres20

Differentiation of rangeland vegetation and assessment of its status: field investigations and MODIS and SPOT VEGETATION data analyses

R. Geerken [a] , N. Batikha [b] , D. Celis [b] & E. DePauw [b]

[a] Department for Geology and Geophysics , Yale University , New Haven, CT 06520, USA

[b] International Center for Agricultural Research in the Dry Areas (ICARDA) , Aleppo, Syria

Published online: 29 Mar 2010.

To cite this article: R. Geerken , N. Batikha , D. Celis & E. DePauw (2005) Differentiation of rangeland vegetation and assessment of its status: field investigations and MODIS and SPOT VEGETATION data analyses, International Journal of Remote Sensing, 26:20, 4499-4526

To link to this article: http://dx.doi.org/10.1080/01431160500213425

International Journal of Remote Sensing
Vol. 26, No. 20, 20 October 2005, 4499–4526

Taylor & Francis
Taylor & Francis Group

Differentiation of rangeland vegetation and assessment of its status: field investigations and MODIS and SPOT VEGETATION data analyses

R. GEERKEN*†, N. BATIKHA‡, D. CELIS‡ and E. DEPAUW‡

†Department for Geology and Geophysics, Yale University, New Haven, CT 06520, USA

‡International Center for Agricultural Research in the Dry Areas (ICARDA), Aleppo, Syria

(*Received 4 May 2004; in final form 16 June 2005*)

In the Syrian Steppe we carried out a field experiment using repeated hyperspectral measurements throughout the 2001 growing season to investigate the separability of vegetation types based on their temporal-spectral signatures. We studied two different perennial shrubs and annual grasses showing differences in the length of their growing period. These differences cause seasonal variations in spectral plant reflectance, also giving hints to functional vegetation characteristics such as palatability, soil stabilization or certain hydrometeorological characteristics. By submitting biophysical and spectral data to statistical analyses we identified the dry season period as the most suitable to discriminate between the studied plants or their functional characteristics respectively. NDVI time series using MODIS or SPOT VEGETATION NDVI bands perform nearly as well as an optimum narrow banded index. For a balanced assessment of the biomass from different functional vegetation groups, our study recommends a narrow banded (9 nm width) vegetation index that uses the 630 nm band together with the 755 nm band. Its particular advantage, compared with indices calculated from MODIS and SPOT VEGETATION bands, is the better correlation with biomass from annual grasses. Conclusions from the field experiment were tested for their transferability to remote sensing conditions. Using the noise-filtered shapes of NDVI cycles as a primary classifier, we identify the distribution and the fractional cover of species with an extended growing period. Pixels with a dominant cover of species with an extended growing period were classified by correlating a reference NDVI cycle with all image pixels, where the calculated correlation coefficient is the measure for shape similarity, and the corresponding slope value the measure for vegetation cover relative to the reference.

1. Introduction

Since dry-land degradation has been recognized as a process that limits the affected countries' agricultural productivity, hampering economic growth or jeopardizing food supply and public health, there is a growing interest in improving the

*Corresponding author. Email: roland.geerken@yale.edu

International Journal of Remote Sensing
ISSN 0143-1161 print/ISSN 1366-5901 online © 2005 Taylor & Francis
http://www.tandf.co.uk/journals
DOI: 10.1080/01431160500213425

assessment and monitoring of parameters that define the status of dry-land ecosystems. Efforts have been focused on the detection of areas that are undergoing rapid changes (Weiss *et al.* 2001, Evans and Geerken 2004) and on understanding the causes responsible for these changes (Pickup *et al.* 1998, Geerken and Ilaiwi 2004). Many approaches use satellite data because often these are the only source of spatial information about these ecosystems, especially about their condition in the past. Also, it is a quick and cost-effective way to assess large areas.

One of the difficulties in using remote sensing data is understanding how, if at all, conventional field indicators that define, for example, vegetation degradation are reflected in the satellite-acquired spectral information. Temporal changes identified by comparing some kind of green-biomass-sensitive vegetation index such as the normalized difference vegetation index (NDVI) measured at different times (Tucker *et al.* 1991, Weiss *et al.* 2001, Evans and Geerken 2004) might not always be a sufficient criterion for labelling an area as degrading or improving. In Middle Eastern and in North African dry-lands, it is not so much the greenness of the vegetation cover that defines ecosystem health but rather the biodiversity, vegetation coverage and functional vegetation characteristics such as palatability or erosion control (LeHouérou 1996). A change or, better, a variation in green biomass may be solely triggered by inter-annual climate fluctuations (Tucker *et al.* 1991, Evans and Geerken 2004) without affecting an area's potential for biomass production. The typically high NDVI values over grassy areas may also lead to wrong conclusions, particularly in areas where perennial shrubs (typically showing low NDVI values) are replaced by annual grasses. In the Middle East and in North Africa, shrubs are valued as a fodder resource, for their contribution to the stabilization of fragile soil systems, for their function in capturing wind-blown seeds, and for increasing water infiltration (Nordblom *et al.* 1996, El-Bana *et al.* 2003, Dunkerley 2000). A clear indicator for a change in the natural resources (degradation/rehabilitation) would be evidence of a change in perennial shrub coverage or in species composition.

The challenge in detecting and differentiating range shrubs using spectral vegetation indices (VI) lies in their scattered distribution, their low level of green biomass, and their occurrence in combination with VI-dominating annual grasses. A number of examples document how shrubs can be mapped from multi-spectral data using spectral indices (Duncan *et al.* 1993), from AVHRR NDVI time series using unsupervised classification techniques (Peters *et al.* 1997) or from multi/hyperspectral data using spectral mixture analysis (Lewis 2000, Okin *et al.* 2001).

It was one of our objectives to discriminate between distinct range vegetation covers. For this we focused on differences in the plants' seasonal phenology or rather the latter's impact on the plants' temporal spectral characteristics. We investigated the spectral cycles of selected species in the field by repeatedly measuring their spectral reflectance throughout a greater part of the season. The temporal-spectral information was then analysed for its potential to discriminate distinct vegetation types and related functional characteristics. Our interest was to test vegetation indices calculated from different wavelength combinations, and particularly to study the shapes of their temporal cycles for their potential to discriminate between perennial shrubs and annual grasses. Further, we assessed the biomass of selected species and the best method and wavelength(s) for its estimation. Finally, we applied our findings to satellite-acquired spectral time series to test their applicability under remote sensing conditions.

2. Methods

We established five monitoring sites in the Aleppo Steppe of Syria (figure 1). Typically, the vegetation cover is dominated by the low palatable woody shrub species *Noaea mucronata* (Rae *et al.* 2001), which grows in combination with different kinds and amounts of annual grasses. *Noaea mucronata* in this study is representative of a larger group of degraded, low palatability or unpalatable dwarf shrubs (e.g. *Cornulaca setifera, Astragalus* sp.) that is characterized by an extended growing period lasting into the dry season. Less widespread, but dominant in a couple of protected plots and in open rangelands, is the palatable woody shrub *Artemisia herba alba*, which also occurs in combination with annual grasses. Because of their nutrient richness, *Artemisia* and annual grasses are a preferred fodder resource for sheep, the dominant ruminant in the Middle East. In contrast to *Noaea*, *Artemisia* does not have an extended growing period, an attribute it shares with many other fodder shrubs that typically grow in the Middle East and in Northern Africa (e.g. *Salsola vermiculata*). Another common feature of these palatable shrubs is their exposure to overgrazing and their increasing replacement by less-desired species (Rae *et al.* 2001).

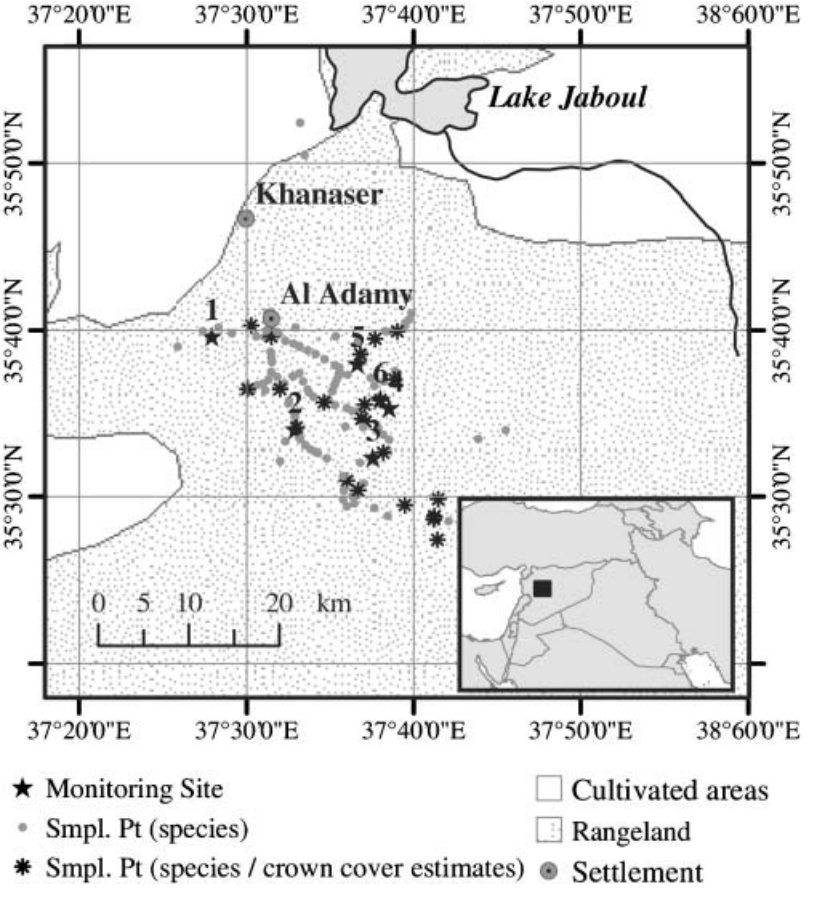

Figure 1. Location map.

We chose two sites within each of the described plant associations plus an additional site where the vegetation cover is solely composed of annual grasses. The individual shrubs that were selected for repeated spectral readings at each site were chosen randomly and marked. To learn about spectral-temporal differences between shrubs and their background we further marked three quadrats of 1 m^2, located between the widely spaced shrubs. Materials summarized in the term 'background' include soil, annual grasses, moss, lichens, pebbles and litter. Their individual contribution to the background signal varies over a growing season. Likewise, three 1 m^2 quadrats were established at the site with only annual grasses. The sites were visited at more or less weekly intervals between 25 February and 5 June 2001. After 5 June, which falls in the dry season and represents a period with no short-term changes in plant phenology, we switched to monthly intervals until the field experiment was completed on 17 September 2001.

During each visit, we took spectral readings using an ASD FieldSpec Pro FR instrument covering the spectral range between 350 and 2500 nm at an interval of 1 nm. Readings were taken relative to a Spectralon white reference. To study seasonal variability in reflectance–biomass relationships, the experiment required the repeated measuring of spectral and biophysical parameters of the same site. This included a non-destructive assessment of the amount of green biomass during each visit. For the shrubs we used the mean length of shoots (current season's growth) (Thalen 1979), averaging five to 10 measurements depending on shrub size. To monitor seasonal biomass variations of the background, we took photographs of each quadrat during each visit (figure 2). To correct photographs for temporal differences in brightness, each photograph included the Spectralon white reference. A colour separation was applied to produce three-layer images (blue, green and red) that were then classified into relevant classes. The area classified as green vegetation is synonymous with the leaf area index (LAI). To translate computed LAIs into aerial biomass we established a reference correlation between LAI and green biomass. For the reference, grasses were clipped from ten 1 m^2 quadrats at each site, three times during the observation period. The oven-dried green biomass obtained from the grasses was then correlated with the LAI analysed from the photographs

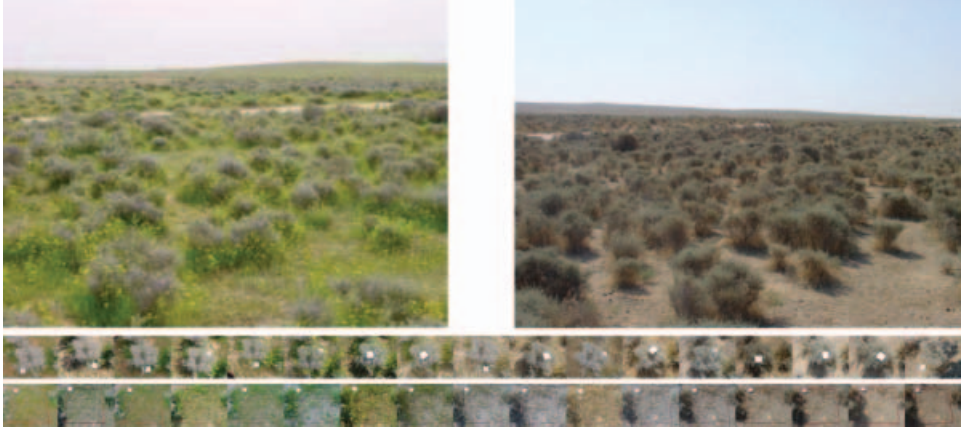

Figure 2. Study site 1 (for location see figure 1) during vegetation peak-time and during the peak of the dry season. Small photographs show seasonal changes for a *Noaea* shrub (upper series) and for its background (lower series).

(R^2=0.89). Only one time series of photographs was analysed for each vegetation combination due to the labour-intensive nature of the evaluation process.

We further measured shrub density and shrub coverage using the line intercept method (Thalen 1979), where shrubs were counted along a transect whose length depended on shrub density (SD). This, together with the average shrub crown cover, approximated from the shrub's longest axis (D_1) and its shortest axis (D_2), allows the calculation of shrub coverage ($SD \times ¼ \times \pi \times D_1 \times D_2$). These data were used for scaling and correlating field results to information from remotely sensed images.

In the course of the experiment, we acquired a total of 4100 spectra that we submitted to statistical analyses to explore spectral-temporal differences between distinct vegetation and/or surface types. Data covering wavelength ranges of reduced atmospheric transmittance (around 1400 nm and around 1900 nm), of limited use for terrestrial remote sensing, and those affected by instrument noise ⩾2400 nm) were omitted from the spectral analyses. It bears mentioning that spectral readings at an individual site could not always be taken at identical sun angles throughout the measuring period. Therefore, we cannot exclude modifying influences on reflectance caused by varying sun elevations (Qi *et al.* 1995a). A smaller number of spectra are affected by cloud coverage, haze or soil moisture, especially some spectra that were acquired in the mornings of our first visits. Those spectra have either been omitted from the evaluation or their impact will be explained where necessary. Spectral readings of each target were taken from three different heights (50, 100 and 150 cm). The fore optic used with the instrument has an 18° field of view that, depending on the measuring height, yields an observed area of 0.0197, 0.0788 or 0.1773 m^2, respectively. To minimize spectral background influences in spectral readings taken from the shrubs, our evaluation of their spectra concentrated on those acquired from the two lower heights. However, as typical for these dwarf shrubs (maximum height is around 50 cm), their branches and leaves do not form a dense canopy, which means some background interference is unavoidable.

The study was carried out in the Aleppo Steppe, which is part of the Syrian drylands. The area receives an average annual rainfall of 200–220 mm and is classified as semi-arid (UNEP 1992). The rainfall season typically lasts from October to March, with maximum precipitation occurring during January/February. The summer season is absolutely dry. The dominant soil type in the Aleppo Steppe is gypsiferous silt, whose spectrum (figure 3) may differ substantially due to variable amounts of pebbles of different materials (flint, carbonate, basalt, gypsum). Abundance of pebbles is minor in areas with perennial shrub coverage, but may be significant in areas with sparse, ephemeral vegetation cover, where pebbles are exposed through deflation of the finer materials. This changes the reflectance intensities and other spectral features (Huete *et al.* 1985).

Because our measurements were mainly concentrated on shrub-grown areas, with a focus on the intra-annual spectral changes, we did not look further into the spectral impacts of soil reflectance. Background features that included lichens, and especially mosses, were more of a problem due to their rapid green-up after rain events and their likewise quick return to dormancy when conditions became drier. This caused misleading correlations between the green biomass measured for the annual grasses, and the acquired spectral reflectance. To avoid dealing with too many variables, quadrats showing this kind of influence were omitted from the analyses. Rainfall amount and distribution are additional parameters that do have

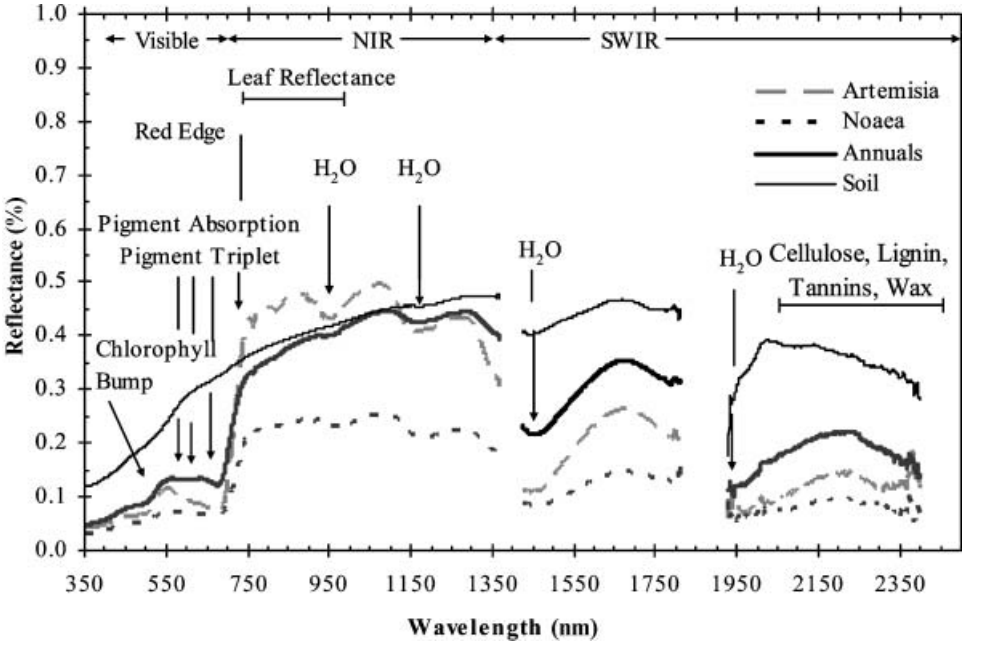

Figure 3. Spectral reflectance of plants (measured at green peak) including materials and plant characteristics triggering reflectance and absorptance.

an influence on vegetation growth, as does soil moisture availability. To ensure that monitored vegetation cycles were a reflection of a certain vegetation type, and not the result of specific growing conditions or of local rainfall events, the monitoring plots were distributed over a smaller area for the experiment, with their soil moisture being sampled at different depths during each visit. We further ensured that soil profiles, and especially their gypsum content (FAO 1990), were comparable between sites so that soil influences were minimized.

3. Data analysis and results

Figure 3 depicts the primary absorption and reflection features of plants in the spectra we acquired. A more complete listing of features and materials is given by Elvidge (1990). Initially we analysed the spectra for characteristics that can be used to differentiate between the monitored vegetation types. Spectral differentiation of shrubs from their background and of the two shrub species from one another were of particular interest.

3.1 *Diagnostic time period(s)*

To describe spectral-temporal differences between chosen vegetation types, we used a simple linear regression calculation technique, in which the correlation coefficient is a measure for the similarity/dissimilarity of the shape of two vegetation spectra. Slope values indicate differences in reflectance (Geerken *et al.* 2005). For example, we correlated a shrub spectrum with the spectrum of its background acquired at the same time. Doing so for each time step creates a time series of correlation coefficients that describes temporal variations in the spectral similarity of the two targets. Figure 4(*a*)–(*c*) shows time series of spectral-temporal similarities between

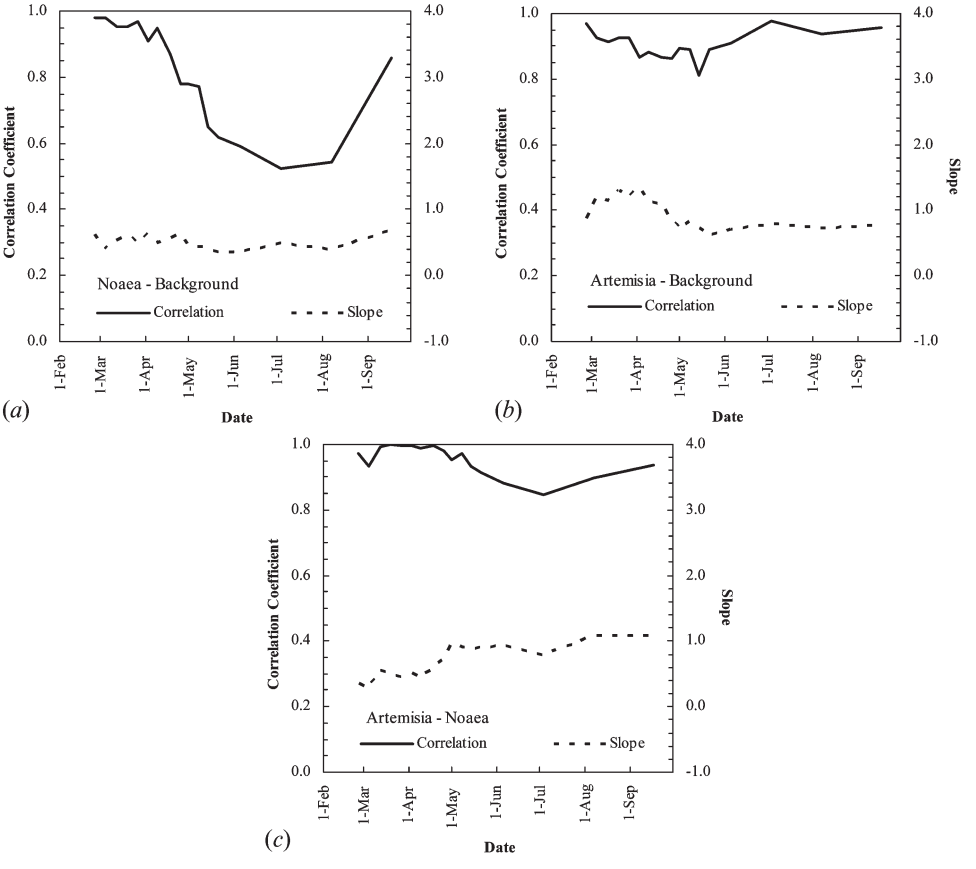

Figure 4. Time series of correlation coefficients and slope values calculated between temporal spectra of *Noaea*–background (*a*), between *Artemisia*–background (*b*) and between *Artemisia–Noaea* (*c*).

Noaea–background, between *Artemisia*–background and between *Artemisia–Noaea*. The *Noaea*–background graph in figure 4(*a*) shows strong similarities during spring time and decreasing similarities starting in mid-April right after the vegetation peak. Similarity reaches a minimum in July/August, representing the hottest period of the year. With correlation coefficients as low as 0.52, the time from June to August appears to have the most diagnostic value to differentiate *Noaea* shrubs from a background of annual grasses. Differences in reflectance intenisties, as expressed in the corresponding slope values, fluctuate around 0.5 to 0.6 without showing a specific tendency. Lower reflectance values are those measured for the *Noaea* shrub (shrub=dependent variable *y*, annuals=independent variable *x*). A slope value of 1 would describe quasi-equal reflectance values for the two vegetation types. *Noaea*'s extended growing period (Rae *et al.* 2001) is crucial for its spectral separability from the background. This triggers high reflectance values in the near-infrared (NIR) range, also causing its NDVI, which is calculated as a ratio from the NIR and red wavelength bands (see equation 1), to remain relatively high throughout the season compared with the NDVI of its background (figure 5).

Unlike the *Noaea*–background plant association, spectral-temporal differences between *Artemisia* and its background are less distinct (figure 4(*b*)). Correlation

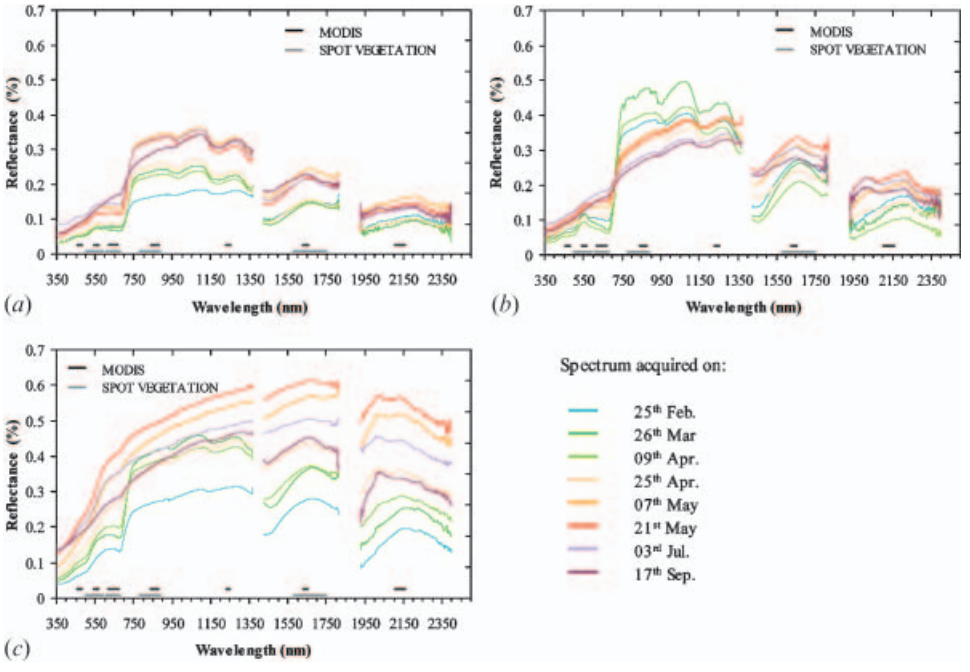

Figure 5. Spectral time series taken from *Noaea* shrubs (*a*), from *Artemisia* shrubs (*b*) and from background material (annual grass, soil, pebbles, litter) (*c*).

values vary between 0.8 and 0.99, showing only minor deviations from a perfect match of the shapes of their spectra during any time of the year. Differences in reflectance, as shown by the slope values, are more pronounced, yielding overall higher values (around 1.25) for *Artemisia* (dependent variable *y*) during the wet spring season but lower values (around 0.8) during the dry summer season. Changes in reflectance can be explained by the increasing spectral influence of high-reflecting background soils, once grasses begin to wilt and the soil becomes increasingly exposed.

The overall similarity in spectral-temporal characteristics of the annual grasses (background) in all sites already highlights the differences found between the two shrubs. Similar to the *Noaea*–background association, regression calculations between the temporal spectra of *Artemisia* and *Noaea* show a similar but less pronounced time curve of correlation coefficients, with a continuous drop-off starting during April, reaching a minimum in June/July (correlation coefficient=0.84) and rising again towards September (figure 4(*c*)). Overall, the temporal-spectral changes displayed by the two shrubs are very similar in trend as the high correlation coefficients reveal, though different in their magnitudes as apparent in figure 5(*a*) and (*c*). As was true for the *Noaea*–background association, the period from June to August also has the most diagnostic value to differentiate between *Noaea* and *Artemisia*. However, the spectral differences are considerably lower than those of the *Noaea*–background association.

The analyses show that the spectral differences between species with an extended growing period, such as *Noaea*, and species without an extended growing period, such as annual grasses or *Artemisia*, are most distinct during the dry period. Evaluations of remote sensing data should concentrate on images taken during this

period. As high correlation values suggest, the temporal differences in the shape of spectra curves from *Artemisia* and its background of annual grasses seem not to offer a very reliable tool to distinguish between the two vegetation types. Described differences in reflectance intensities do not adequately separate *Artemisia* shrubs from a grassy background because these differences can also be an expression of vegetation cover variations or plant vigour variability.

3.2 *Diagnostic wavelengths*

The above correlation calculations are used as a measure for the overall similarity of the shapes of spectral curves from different vegetation covers considering their similarities/differences over time. To figure out the exact wavelengths that are triggering these dissimilarities, we looked further into the temporal-spectral changes related to the various vegetation covers. In contrast to previously discussed diagnostic time period analyses, we next correlated two time series of reflectance values measured at the same wavelength. Repeating this for each wavelength gives one correlation coefficient for each wavelength, describing how similarly two targets develop through time at a specific wavelength. We compared both shrub types with their grassy background and the two shrubs with each other (figure 6). Spectra in figure 5 help explain temporal-spectral correlations between the investigated plant species. Elements common to all three species are increasing reflectance values in the mid-infrared with increasingly dry conditions; however, changes occur at considerably different rates, underscoring the plants' individual water management capabilities. All species show a uniform drop in reflectance throughout all wavelengths after reaching their maximum reflectance around mid-May (figure 5).

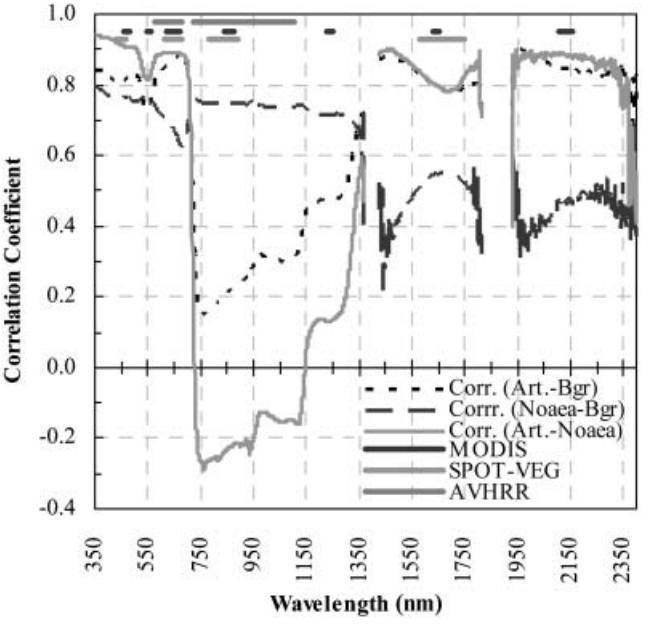

Figure 6. Correlation of spectral time series calculated between *Noaea*–background, *Artemisia*–background and *Artemisia–Noaea.* Spectral bands of high temporal resolution sensors are indicated at the top.

While *Noaea* reflectance in the NIR range increases continuously from February until its peak (maximum NDVI calculated from the field-measured spectra using MODIS NDVI bands) at the beginning of April and further increases thereafter, *Artemisia* NIR reflectance is near its highest from the very beginning of our measurements, showing some fluctuations in reflectance until reaching its green peak at the beginning of April. After the April maximum, NIR reflectance starts to drop.

With correlation values at around 0.78, *Noaea* and its background display relatively uniform spectral changes in the visible and NIR range. Exceptions are the wavelengths around 681 nm, next to the red edge, where lower correlation coefficients indicate higher dissimilarities in the temporal development of spectral reflectance. The reason for this can be found in the vegetation-characteristic red edge, which changes to a convex shape in the case of the background material as dryness increases but remains a pronounced concave feature in the *Noaea* spectra (figure 5(*a*) and (*c*)). In the mid-infrared range, correlation coefficients drop to values around 0.5 with absolute lows of 0.4 to 0.3 towards the water absorption bands (OH^- and H_2O) near 1400 nm and near 1900 nm. This is due to differences in the plants' water conservation abilities, differences in plant materials (woody shrubs) and the variable influence and contribution of high-reflecting soil to the background signal that trigger the seasonal-spectral differences in the mid-infrared wavelength range.

Dissimilarities in the seasonal cycle of *Artemisia* and its background are highest in the NIR range (figure 6). This is caused by the broader leaves of *Artemisia* and its denser green canopy triggering high NIR reflectance values during the growing period that suddenly drop when wilting sets in. Coinciding with the loss in greenness is the exposure of the dark woody material. At the same time, the NIR reflectance of the background rises with increasing grass growth and remains at a high level or increases even further during senescence (figure 5(*b*) and (*c*)). It is due to the growing influence of the soil that the NIR reflectance of the background is kept at a high level, leading to lower *Artemisia*–background correlation coefficients in this wavelength range (figure 6). Correlations throughout the mid-infrared are high, as a result of a consistent rise in reflectance with increasing dryness, visible in both plants. Again, the changes in reflectance are attributed to variations in materials contributing to the spectral signal (green biomass, woody materials and background components) but also to the loss of plant water. The high reflectivity of the wilted grass material is another reason for the continuous rise in spectral reflectance after the vegetation peak. Reflectance values start to drop after removal of the grass residues. In our observations, we measured a typical soil reflectance about 2 months after the vegetation peak (figure 5(*a*)–(*c*)). By this time most of the grass residues had disintegrated or been deflated.

The same opposing trends in NIR reflectance measured between *Artemisia* and *Noaea* and as described above for *Artemisia* and background material (figure 5), are responsible for low correlation values in the NIR range (figure 6). Minor dissimilarities in the two shrubs' temporal-spectral development are found in the visible with a maximum at 550 nm. This applies similarly to the mid-infrared range where high correlation coefficients indicate comparable temporal trends. As can be seen in figure 5 and as becomes clear from analysing the corresponding slope values (not shown), absolute differences in reflectance values in the mid-infrared are, however, considerably higher than those in the visible.

3.3 *Vegetation index cycles*

The analyses described above indicate that there are diagnostic spectral differences that make it possible to distinguish between vegetation with an extended growing period and vegetation without an extended growing period. A diagnostic signal within a temporal cycle is most diagnostic if analysed in context with the cycle within which it occurs. Also, other than the optimum single spectral band, it was the objective of our analyses to identify the optimum two-band ratio index. Most indices use a ratio composed of bands from the NIR wavelength range and from the red wavelength range in which vegetation shows a characteristic reflectance contrast (Richardson and Wiegand 1977, Huete 1988, Qi *et al.* 1995b). In addition to their sensitivity to green biomass, ratio indices are especially valued for their smoothing effect on noise (e.g. caused by atmospheric variations, topography or sensor noise). As representative for other indices, we used the NDVI formula (equation 2) to identify the two-band ratio cycle (wavelength position/width) that enhances best the temporal-spectral differences between the two vegetation types—under the assumption that the same spectral bands would perform similarly well or poorly in most other two-band vegetation indices. In contrast to the NDVI, we also looked into wavelength combinations including the frequency range of the mid-infrared, where variations in water content are visible. Accordingly, we calculated normalized ratio time series from our field measured spectra for *Noaea*, for *Artemisia* and for the background, using all possible band combinations between 400 nm and 2399 nm.

$$\mathrm{NDVI} = \frac{\mathrm{NIR} - \mathrm{Red}}{\mathrm{NIR} + \mathrm{Red}} \tag{1}$$

$$\text{Ratio index}_{x,\,y} = \frac{X_{(400-2398)} - Y_{(401-2399)}}{X_{(400-2398)} + Y_{(401-2399)}} \tag{2}$$

We also correlated the ratio time series calculated for *Noaea* with those calculated for the background to identify the ratio index that best enhances differences in their vegetation cycles. The same calculation was done between *Artemisia* and its background and between *Noaea* and *Artemisia*. The diagrams in figure 7(*a*) and (*b*) show the results of two out of three plant combinations, with the *xy*-position indicating the wavelengths used for ratio calculation and the colour standing for the correlation coefficient calculated between two normalized ratio cycles. For reasons of clarity, figure 7 only shows ratio combinations calculated from the visible and part of the NIR range. Plots covering the full wavelength range (400–2399 nm) are available upon request from the authors.

Basically, the lower the correlation coefficient the more dissimilarly the two ratio cycles develop over time. However, the conclusion that lower correlation values indicate a more diagnostic band combination is not necessarily correct. The lowest correlation values (around −0.5) as calculated for some SWIR–SWIR (shortwave infrared) and for some visible–red edge (700–750 nm) band combinations, for example, display only minor differences in absolute values between the two ratio cycles. These typically range within the noise level of operational sensors and for this reason cannot be radiometrically resolved. Also, the spectral changes and trends visible in the SWIR range are very complex and difficult to relate to their particular origin, especially where background material forms one variable. They often may be triggered more by background influences than by plant-typical phenological

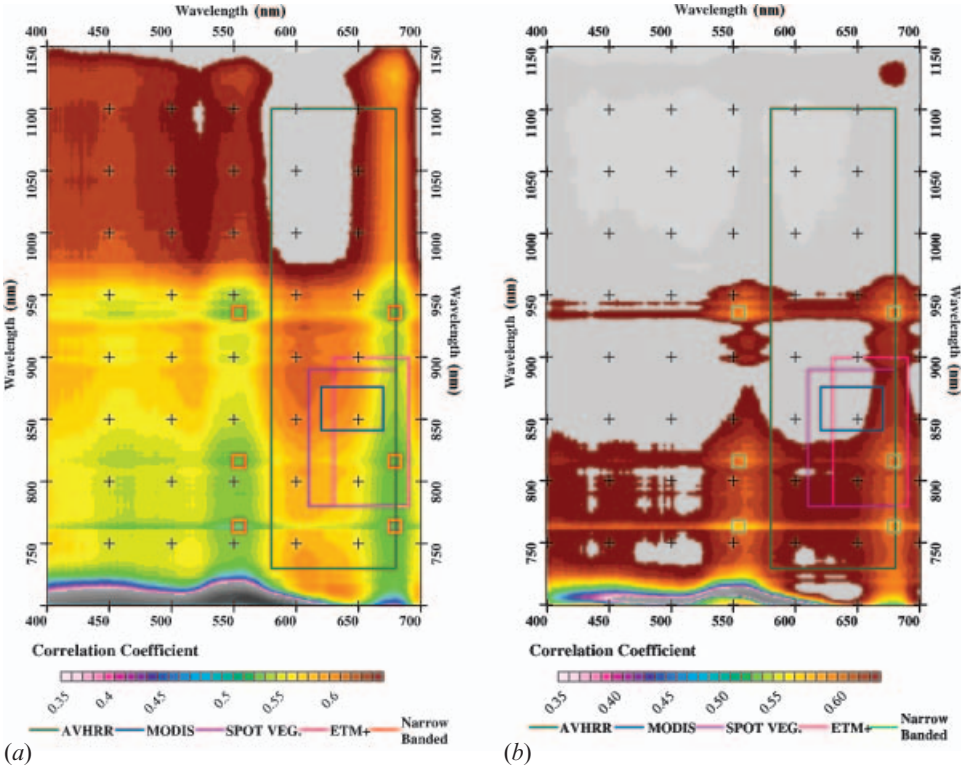

Figure 7. Correlation coefficients calculated between time series of normalized two-band spectral ratio indices of *Noaea* and of background (*a*), and of *Noaea* and of *Artemisia* (*b*). Ratios were calculated at 1 nm steps. Band combinations with correlation coefficients higher than 0.65 (light grey) and lower 0.35 (dark) are in grey scale.

changes. A possible background influence is the reason why we did not focus on a ratio that enhances SWIR reflectance differences triggered by the plants' water storage capabilities and/or their plant tissue composition (figure 3). Though absolute differences are at a maximum and correlation coefficients between ratio cycles of the more drought-resistant plant *Noaea* on one side and the grasses and *Artemisia* on the other side are among the lowest when using a combination of the 945 nm band (NIR range) with the 2244 nm band (SWIR range) (figure 8(*c*) and (*d*), table 1), low reflectance values in the SWIR band may also be caused by hydrous minerals such as gypsum, a prominent mineral in some semi-arid soils.

In the following analyses we therefore concentrated on ratio indices composed of spectral bands of the visible range and of the NIR range (figure 7(*a*) and (*b*)) where phenological changes are best documented. Overlaid on the correlation values in figure 7(*a*) and (*b*) are the wavelength ranges covered by the NDVI bands of some operational sensor systems and a series of best narrow band ratios, with their discriminating power, expressed in the correlation coefficient, shown in table 1. The optimum narrow band ratio, providing the lowest correlation coefficient (0.509) between *Noaea* and background, was identified as the combination of the 679 nm band with the 764 nm band at a 10 nm band width. The same NIR band in combination with the 554 nm band provides another correlation low (0.511). These band combinations work equally well to discriminate between *Noaea* and *Artemisia*,

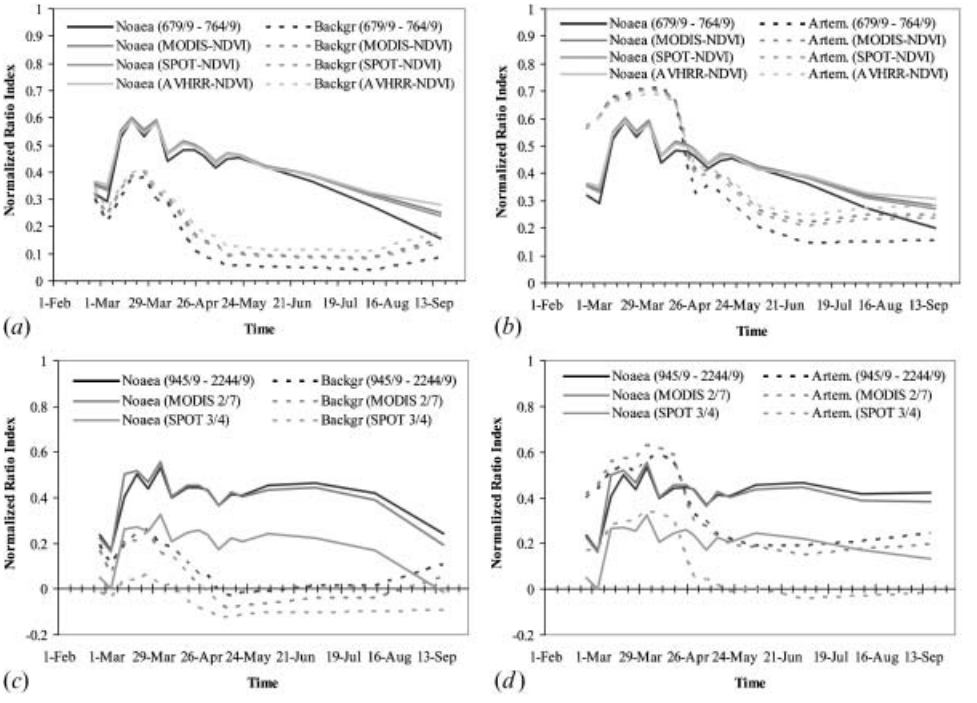

Figure 8. Comparison of two-band ratio time series of *Noaea* and of background materials (*a* and *c*) and of *Noaea* and *Artemisia* (*b* and *d*) using band combinations of the visible with the NIR range (*a* and *b*) or of the NIR with the SWIR range (*c* and *d*), respectively. Bands employed for ratio calculation are specified in the legend of each diagram.

but the optimum band position providing the lowest correlation value (0.592) is obtained by shifting the 554 nm band to 560 nm (table 1).

Discrimination between *Artemisia* and the annual grasses is best during the period immediately after the vegetation peak (figure 4). The reason for this is the somewhat delayed drop in *Artemisia*'s greenness, which reaches a low about 3 months after the green peak (here, at around the end of June) compared with a much quicker loss of green biomass in the case of the background annuals, which reach their green biomass low already about 1½ months after the green peak (here, during mid-May) (figure 8). Simple linear correlation techniques using the entire field-measured time series, however, are not sensitive enough to enhance the short-dated differences. Accordingly, linear correlation calculations between any normalized two-band ratio cycle of the two vegetation types results in strongly correlated cycles for almost all wavelength combinations (not shown). The most strongly correlated ratio cycles are those calculated from a combination of visible with NIR bands.

To discriminate between vegetation with an extended growing period and vegetation without an extended growing period, the analyses suggest an optimum ratio with the red band centred at 679 nm or 550 nm and with the NIR band centred at 764 nm. However, the performance of NDVI bands of high temporal resolution sensors such as SPOT VEGETATION and MODIS is not significantly worse (figure 8 and table 1). In simulations that use the spectral field data, the two spectrally enhance the phenological differences between the two vegetation types equally well so that a reliable discrimination can be expected. Dissimilarities in

Table 1. Correlation between ratio (NDVI) cycles of *Noaea* shrubs and of annual grasses and between *Artemisia* shrubs and *Noaea* shrubs for visible–SWIR band combinations.

Narrow band combinations (9 nm band width)									
Wavelength combination (nm):	560/764	560/817	560/936	679/764	679/817	679/936	945/2244	1143/2244	1349/2244
Between *Artemisia* and *Noaea* normalized ratio cycles	0.592 (0.016)	0.611 (0.004)	0.605 (0.006)	0.603 (0.008)	0.613 (0.002)	0.610 (0.004)	0.052 (0.012)	0.022 (0.014)	**−0.060 (0.020)**
Wavelength combination (nm):	554/764	554/816	554/936	679/764	679/816	679/936	945/2244	1143/2244	1349/2244
Mean Corr. Coeff. (StDev) calculated between Background and *Noaea* normalized ratio cycles	0.511 (0.012)	0.525 (0.003)	0.530 (0.005)	0.509 (0.008)	0.519 (0.002)	0.529 (0.004)	−0.036 (0.010)	−0.047 (0.012)	**−0.120 (0.018)**

Band combinations from temporal high-resolution sensors									
Sensor:	MODIS					SPOT VEG.			AVHRR
Band combination:	3/2	4/2	1/2	2/7	5/7	1/3	2/3	3/4	1/2
Between *Artemisia* and *Noaea* normalized ratio cycles	0.665 (0.004)	0.646 (0.006)	0.656 (0.009)	**0.233 (0.030)**	0.247 (0.038)	0.656 (0.010)	0.646 (0.015)	0.285 (0.056)	0.664 (0.028)
Between Background and *Noaea* normalized ratio cycles	0.565 (0.004)	0.554 (0.005)	0.583 (0.018)	**0.114 (0.022)**	0.132 (0.032)	0.559 (0.010)	0.571 (0.025)	0.156 (0.052)	0.602 (0.040)

Ratios with the highest discriminating power (sensor bands and best-performing narrow bands) are shown in bold. Presented correlation coefficients are calculated as the mean from correlation calculations done at 1nm steps.
Values are the mean correlation coefficient (SD).

growing cycles such as were found between *Artemisia* and annual grasses are not strong enough to be resolved with linear correlation methods and may require a different approach.

4. Correlation between biomass and spectral reflectance

A number of studies have been undertaken to investigate the best approach to describe biophysical parameters such as LAI or percentage green cover in arid and semi-arid environments. Huete and Jackson (1987) and Elvidge and Chen (1995) discuss the advantages of the various vegetation indices, either ratio index (e.g. NDVI) or orthogonal index (e.g. the perpendicular vegetation index (PVI) of Richardson and Wiegand 1977) or a combination of both such as the soil adjusted vegetation index (SAVI) of Huete (1988) (equations 3 and 4). Both studies conclude that orthogonal indices or hybrid VIs perform better in sparse vegetation covers than ratio indices. Elvidge and Chen (1995) demonstrate the strong correlation between a first-derivative-based green vegetation index (DGVI) and LAI, and the poorer performance of various broad band and narrow band vegetation indices (NDVI, SAVI, PVI). All studies use single-date images, not time series, to establish their correlations between biomass and a specific vegetation index.

$$\mathrm{SAVI} = \frac{\mathrm{NIR} - \mathrm{Red}}{\mathrm{NIR} + \mathrm{Red} + L}(1 + L) \tag{3}$$

$$\mathrm{PVI} = \frac{(\mathrm{NIR} - a \times \mathrm{Red} - b)}{\sqrt{a^2 + 1}} \tag{4}$$

where L=soil adjustment factor (0.5), a=slope of soil line and b=intercept of soil line.

In contrast with the studies of Huete and Jackson (1987) and Elvidge and Chen (1995), which focus on the best approach to assess undifferentiated green biomass in sparsely vegetated areas, it was our intent first to investigate methods to discriminate between distinct vegetation types, and second to assess their individual biomass. Because our classification and biomass assessment approach uses time series rather than single-date data, the selected vegetation index had to be robust to temporal variable noise, which is better accomplished by the NDVI. Another of our goals was to determine how accurately spectral indices can describe mixed vegetation covers composed of different perennial shrubs and annual grasses. We demonstrated that there are phenological differences between certain vegetation types that create diagnostic temporal-spectral signatures. But how well can their individual biomass be approximated using a single-wavelength or a distinct two-band ratio index? To answer these questions we studied the temporal-spectral characteristics of *Artemisia herba alba*, *Noaea mucronata* and the annual grasses (background) together with the plants' particular biomass. We correlated biomass with reflectance from single wavelengths and with two-band spectral indices in order to locate the best-performing wavelengths and wavelength combinations.

4.1 *Single band correlations*

We correlated the spectral reflectance of each vegetation type (*Artemisia*, *Noaea* and grass) with its green biomass to locate the best-correlating single band(s). Biomass

and spectral data used in the correlation calculations cover the period from the beginning of our measurements (25 February) to the peak time of vegetation (end of April), totalling 180 measurements for each shrub type and 45 for the annual grasses. The best-correlating wavelengths for all vegetation types are located in the NIR range between 755 and 762 nm with the waveband at 862 nm also performing well for *Artemisia* (figure 9). *Artemisia* shows high negative correlations around the water bands (1400 and 1900 nm) which emphasizes the plant's less well developed mechanisms to prevent water loss (increasing green biomass is related to a drop of reflectance in the water bands due to water absorption), a sign of its poorer adaptation to dry conditions (Elvidge 1990). In contrast to *Artemisia*, the more drought-resistant *Noaea* does not display a similar significant correlation between biomass and spectral reflectance in its 1400 and 1900 nm water bands. *Artemisia*'s greater need for plant water in order to develop green biomass is also documented in the NIR range (950 and 1100 nm), indicated by a clear drop in values at these positions but only a minor one for *Noaea*. In the red wavelength range, a range used in most vegetation indices, there are considerable differences in biomass–reflectance correlation between *Artemisia* and *Noaea*, caused by pigment absorptions (figure 3). The magnitude of absorption is a matter of the plant's photosynthetic activity, which again can vary considerably depending on the protective mechanisms a plant develops in order to survive under dry conditions (Elvidge 1990). One of those mechanisms is to minimize the photosynthetic activity to control plant temperature (e.g. achieved by reducing the absorption of sunlight). This explains why there is no correlation between *Noaea* green biomass and *Noaea* reflectance in the red wavelength range but a relatively strong negative correlation in the case of *Artemisia* (figure 9). As expected, correlations are lowest for the annual grasses because of a higher influence of other components including soil, lichens and litter, and of episodic green-ups of mosses.

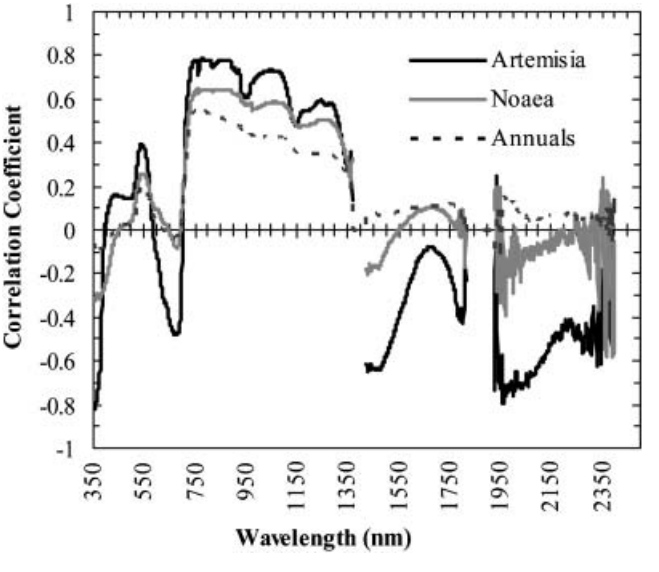

Figure 9. Correlation between green biomass and spectral reflectance.

4.2 *Broad and narrow two-band indices*

To identify the best-correlating two-band ratio, we calculated all possible combinations of normalized two-band ratios between 350 and 2399 nm (see equation 1) and correlated each ratio time series with the corresponding green biomass (figure 10). As in the single-band analysis, we used the data collected between 25 February and the peak time of vegetation. The result shows a number of contrary features between *Artemisia* and *Noaea*. While a combination of a NIR band (between 750 and 950 nm) with a band centred at around 550 nm (wavelength of reduced chlorophyll absorption) gives a correlation maximum for *Noaea* it forms a low in the case of *Artemisia*. Similar opposing correlation relationships are noted for a number of additional wavelength combinations whereby a local correlation maximum for one species is a minimum for the other, for example the previously mentioned NIR band in combination with either of these bands: 740 nm (red edge), or 950 nm, or 1500 nm or 1750 nm. *Artemisia* clearly shows elongated local maxima (when used in combination with a broad NIR band) or local minima (when used in combination with a broad visible band) in correlation coefficients at the water absorption bands (950 and 1150 nm), emphasizing the plants' water needs for biomass production. In contrast, a relationship between biomass and water features is barely visible in any two-band ratio/*Noaea*–biomass correlation. This difference in biomass–water dependency is further documented by strong *Artemisia* correlations in mid-infrared band combinations compared with very weak *Noaea* correlations in the same band combinations.

Clearly, trying to find the best-correlating band combination for one species often is at the expense of the other. While there are a number of NIR–NIR narrow band combinations showing good biomass correlations for both species, such wavelength combinations lack the vegetation diagnostic information offered by the contrast between the red and the NIR band. Using a single NIR band or a ratio composed of NIR bands only will cause a conflict with the high NIR reflectance of soils in arid and semi-arid areas, except in areas that have already been identified as vegetation-covered prior to any biomass assessment.

The same correlation analyses calculated between the biomass of annual grasses and all possible two-band ratios between 350 and 2399 nm (figure 11(*a*)) resulted in much lower correlation coefficients, with an absolute maximum at 0.75. For clarity, only VNIR combinations are shown; plots covering the full range are available from the authors. In figure 11(*a*), only correlations higher than 0.50 are shown in colours; values below 0.50 are in grey scale with black indicating the lowest correlation coefficients. The pattern of high and low correlation values in figure 11(*a*) is different from that of any shrub, narrowing the possibilities of band combinations that ensure an equally good biomass correlation for all three vegetation types. Except for a small wedge, describing red edge band combinations (centred at around 725 nm/725 nm), all band combinations with stronger correlation are NIR–NIR or NIR–SWIR ratios. The performance of NDVI bands of selected sensor systems in describing green biomass, including two alternative narrow band combinations, are summarized in table 2.

Recalculating visible–NIR band combinations using the SAVI instead of the NDVI (figure 11(*b*)) considerably improved correlations for all wavelength combinations, with the highest values reached in red edge band combinations and in a combination of the 750 nm band with the 515 nm band (correlation coefficient = 0.72). The mean correlation coefficient between green biomass and

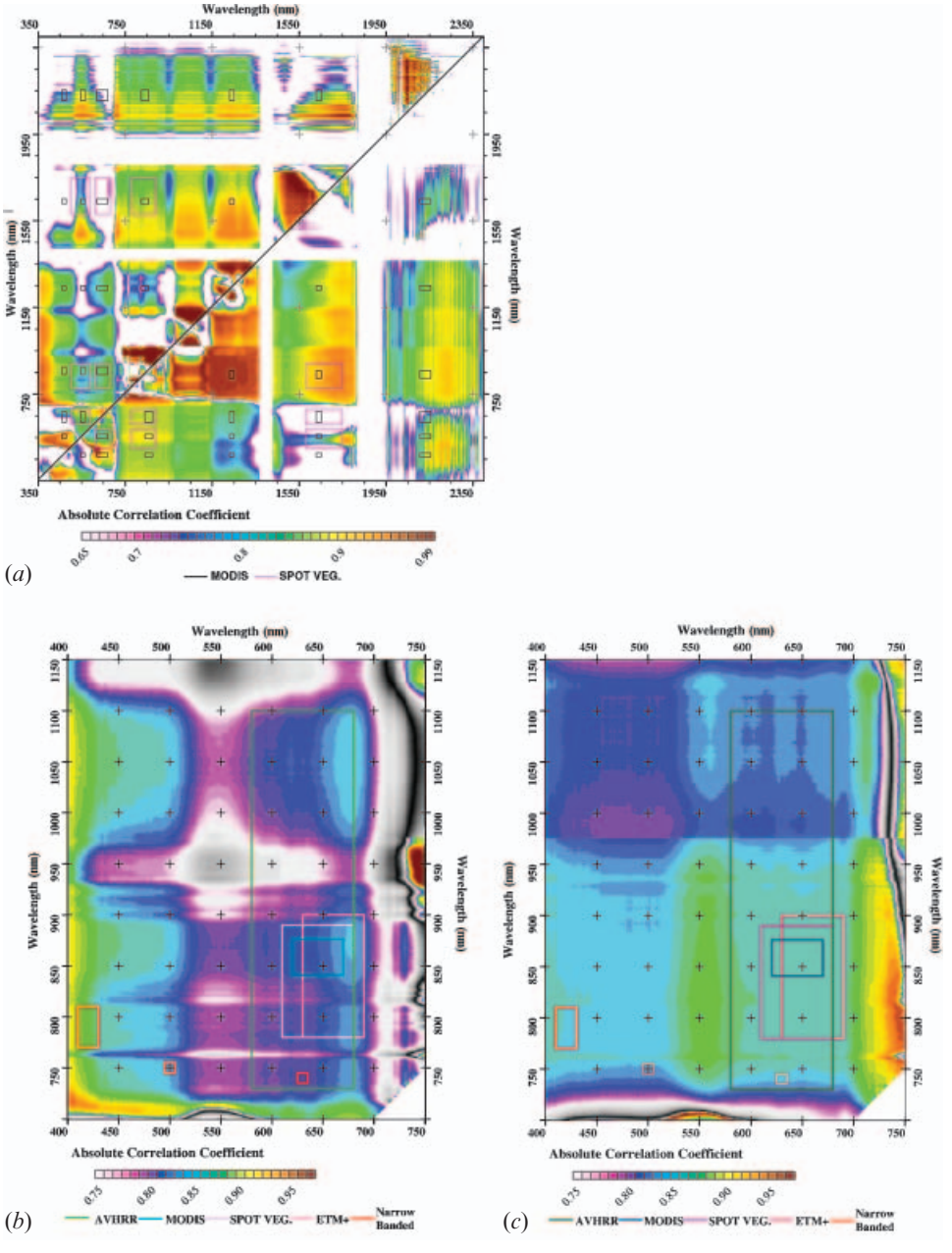

Figure 10. Correlation coefficients calculated between green biomass of *Artemisia* and normalized two-band ratios from *Artemisia* spectra (*a*, triangle above diagonal and *b*, contrast stretched VNIR range) and between green biomass of *Noaea* and normalized two-band ratios from *Noaea* spectra respectively (*a*, triangle below diagonal and *c*, contrast stretched VNIR range). Ratios were calculated at 1 nm steps. Overlaid boxes indicate NDVI bands of selected sensor systems and band combinations that perform best for all vegetation types. Correlation coefficients lower than 0.75 are in grey scale (white indicating higher, black lower correlation values).

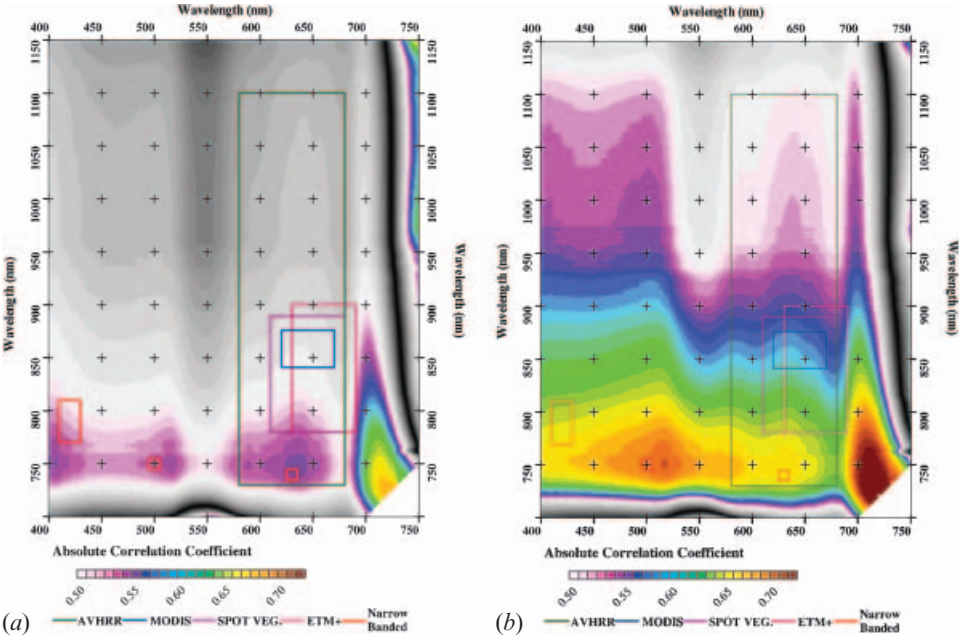

Figure 11. Correlation coefficients calculated between the green biomass of annual grasses (background) and normalized two-band ratios of their spectra using NDVI (*a*) and SAVI (*b*). Ratios were calculated at 1 nm steps. Overlaid boxes indicate NDVI bands of selected sensor systems and band combinations that perform best for all vegetation types. Correlation coefficients lower than 0.50 are in grey scale (white indicating higher, black lower correlation values).

Table 2. Comparison between green biomass/NDVI correlations, with the NDVI calculated from different wavelength combinations, and correlated with different rangeland vegetation types.

	Sensor							
	MODIS			SPOT VEG.		AVHRR	Best performing	
Band combination:	3/2	4/2	1/2	1/3	2/3	1/2	425/29 790/39	415/15 790/39
Artemisia	**0.859**	0.805	0.828	0.858	0.825	0.812	0.853	**0.891**
	(0.002)	(0.003)	(0.009)	(0.007)	(0.012)	(0.040)	(0.001)	**(0.009)**
Noaea	0.847	**0.875**	0.858	0.850	0.858	0.848	**0.875**	0.854
	(0.001)	**(0.001)**	(0.001)	(0.002)	(0.002)	(0.012)	**(0.013)**	(0.002)
Annuals	0.453	0.392	0.468	0.471	**0.480**	0.440	0.514	**0.522**
	(0.006)	(0.013)	(0.010)	(0.022)	**(0.025)**	(0.055)	(0.011)	**(0.009)**
	0.621	*0.582*	*0.590*	*0.632*	*0.605*	*0.563*	*0.657*	*0.656*
	(0.006)	*(0.009)*	*(0.009)*	*(0.020)*	*(0.025)*	*(0.058)*	*(0.007)*	*(0.007)*

Values in italics are those calculated for biomass/SAVI correlations. The band combinations under 'Best performing' are given as centre wavelength/band width (nm).
Correlation/SD of best performing band combination for each vegetation type, distinguished by operational sensors and absolute 'best performing' are indicated in bold values.
Values are mean correlation coefficient (SD).

SAVI calculated from all visible–NIR combinations (400–1150 nm) is 0.556, which is an improvement of 0.143 compared with green biomass–NDVI correlations for the same wavelength range. A comparison of VI performance between the NDVI and the SAVI is presented in table 2 for the annual grasses, for selected band combinations. Green biomass–SAVI correlations were also calculated for both shrubs, but without significant improvement in correlation coefficients. This was to be expected because measurements were merely focused on the shrubs and tried to minimize background influences.

The attempt to find the optimum band combination(s) that describes sufficiently well any of the three studied vegetation types is a trade-off between maximum performance for one vegetation type and lower biomass correlations but quasi-equal performance for all. To narrow down the number of possible wavelength combinations, we first identified the spectral bands that perform equally well for both shrub types. The conditions were defined as follows: the correlation coefficient for each shrub had to be higher than 0.8 and the difference between them had to be less than 0.05. Setting a higher threshold for the correlation coefficient or allowing variation only within a narrower range would have left us only a very limited number of possible wavelength combinations. Wavelengths that fulfil the set conditions are shown in figure 12. Among the visible–NIR band combinations, narrow bands centred at 415 nm/790 nm and 425 nm/790 nm give the highest correlations for both shrubs (table 2) with a difference between them that falls within the defined 0.05 threshold. With the correlation values for the annuals not at their highest (NDVI=0.522 and 0.514 respectively or SAVI=0.656 and 0.657) this might

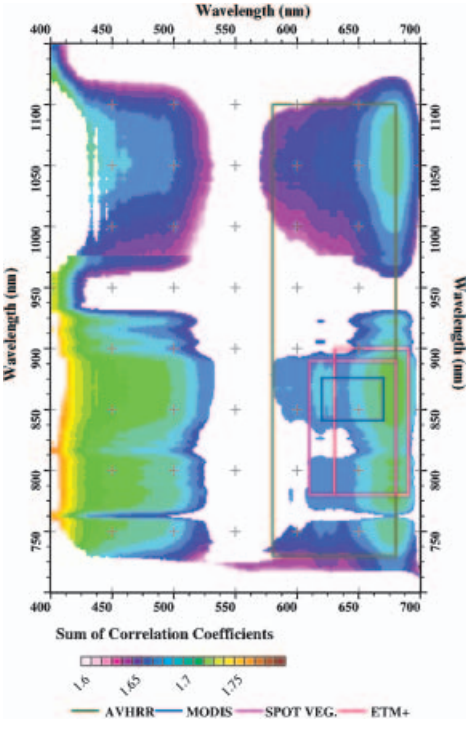

Figure 12. Wavelength combinations of best-correlating normalized two-band ratios with both *Noaea* green biomass and with *Artemisia* green biomass.

Table 3. Wavelengths and biomass correlation of a two-band vegetation index that performs equally well for all studied vegetation types.

	Band centre/width (nm)			
Vegetation type	505/9 755/9 (NDVI)	505/9 755/9 (SAVI)	630/9 755/9 (NDVI)	630/9 755/9 (SAVI)
Artemisia herba alba (shrub)	0.837 (0.007)		0.858 (0.002)	
Noaea mucronata (shrub)	0.843 (0.004)		0.813 (0.002)	
Annual grasses	0.536 (0.004)	0.696 (0.003)	0.550 (0.002)	0.671 (0.001)

Values are correlation coefficient (SD).

not be the optimum choice, especially not where annuals are the dominant vegetation type as is often the case in arid and semi-arid environments. These band combinations might also prove to be of little diagnostic value because of similar reflectance ratios measured for the high-reflecting soils typical for arid regions (figure 3). A prior identification of an area as 'vegetation-covered' would be required before assessing biomass production, in order to exclude ratio values calculated from the soils. Accepting somewhat lower correlation values for both shrub types (0.837, 0.843), the alternative band combination at 505 nm/755 nm gives a small boost to the annuals' NDVI–biomass correlation coefficient (0.536) and to the annuals' SAVI–biomass correlation coefficient (0.696) (table 3). The optimum red–NIR index according to our criteria is a combination of the 630 nm band with the 755 nm band, which provides correlation values of 0.858 (*Noaea*), 0.813 (*Artemisia*) and 0.550/0.671 (annuals, NDVI/SAVI). The latter two will ensure a more balanced biomass assessment of all three vegetation types and exclude the possibility of confusing soils with green biomass.

5. MODIS and SPOT VEGETATION satellite data analyses

When transferring the results of our field studies to remote sensing data, spectral signatures of shrubs become less clear compared with their field-measured signature. Their scattered distribution, their variable coverage, ranging from about 30% down to 0 ground cover, their coexistence with other species, and the suitability as well as the problems in assessing biomass from sites large enough for up-scaling to 1000 m or 500 m resolution satellite data, affect the purity of the spectral signals and the quality of correlations between satellite-acquired spectral reflectance and distinct biophysical parameters. Having identified a characteristic temporal-spectral signal for shrubs with an extended growing period (such as *Noaea*) and one for range vegetation without an extended growing period (e.g. annual grass and *Artemisia* shrubs), we investigated the vegetation index time series of the MODIS sensor and of the SPOT VEGETATION sensor to test whether we could achieve the same separation based on satellite-acquired vegetation index cycles. We calculated and tested NDVI and SAVI time series of both sensors. The time series cover the hydrological year 2000/2001, starting on 1 October and ending on 31 September. The SPOT VEGETATION time series includes 36 layers (1 October to 21 September): the MODIS500 (Version 4 of MOD09A1) contains 44 layers (Julian Day 281 to Julian Day 273) with two dates missing that are not available. Preference was given to the MODIS 8-day composite over the 16-day NDVI composite to

study the temporal resolution requirements needed for capturing diagnostic features in vegetation growing cycles (Geerken *et al.* 2005).

Because the amplitudes of annual NDVI cycles of a distinct vegetation type will vary as a function of spatial variations in crown cover, in plant vigour or in degradation, we consider supervised or unsupervised classifications as not especially suited to the identification of a class with such variability. Therefore, for the identification of vegetation index cycles with a characteristic temporal distribution of NDVI values, we picked a reference cycle from the satellite image with a known vegetation cover (species, crown cover) and linearly correlated the reference with all image pixels (Geerken *et al.* 2005). The chosen reference site is dominated by shrub species with an extended growing period. The degree of similarity between the reference cycle (X) and the tested cycles (Y) is expressed in the correlation coefficient. The higher the correlation value the higher the probability that an area is dominated by a species with an extended growing period. By admitting only high-correlating pixels, the corresponding slope values can be used as a measure for the assessment of crown cover relative to the reference site. Accepting lower-correlating pixels indicates an increasing influence of other species that will influence the slope values (relative crown covers), restricting their usefulness in coverage assessments. Describing the similarity of NDVI cycles through linear correlation works well as long as vegetation cycles resemble a normal distribution. Linear correlation is not useful in describing similarities between more complex vegetation cycles (e.g. induced by double cropping, or in areas that are temporarily flooded or snow-covered) (Geerken *et al.* 2005).

To prevent temporally and spatially variable data noise from interfering with the degree of similarity, we Fourier-filtered the reference cycle. In an interactive process we applied an individual weight to each magnitude of the reference cycle to eliminate higher-frequency noise while preserving most of the phenological characteristics (figure 13) (Geerken *et al.* 2005). The Fourier parameters that best describe our reference cycle were then applied to the entire data set to build a noise-reduced layer stack. A comparison between the high-frequency magnitudes (5 and higher) of the MODIS reference cycle and those of the SPOT reference cycle (figure 13(*b*) and (*d*)), shows considerably higher values for MODIS, indicating higher noise in the MODIS cycle. But it is especially due to random NDVI spikes between day of the year (DOY) 64 and DOY 128 (figure 13(*a*)) that the phenological features in the MODIS cycle are less well preserved after Fourier filtering compared with the SPOT cycle. NDVI spikes in MODIS are triggered by exceptionally low reflectance values in the red band that were not flagged in the quality control file. In situations in which these spikes are not a consistent feature throughout the analysed data set (do not occur at the same time in all pixels), the assessment of cycle similarities will be affected (Geerken *et al.* 2005).

5.1 *Verification of classification results*

During the verification process, we checked how many of our field locations described as 'shrubs with extended growing period' were correctly identified in our classification. Likewise we cross-checked field locations described as 'vegetation cover with no extended growing period' for the extent to which they were incorrectly attributed to the 'extended' class. By setting a threshold for the correlation value, we defined the minimum similarity requested between reference cycle and tested cycle. Thresholds that gave the best match with our sampling points are 0.97 for MODIS

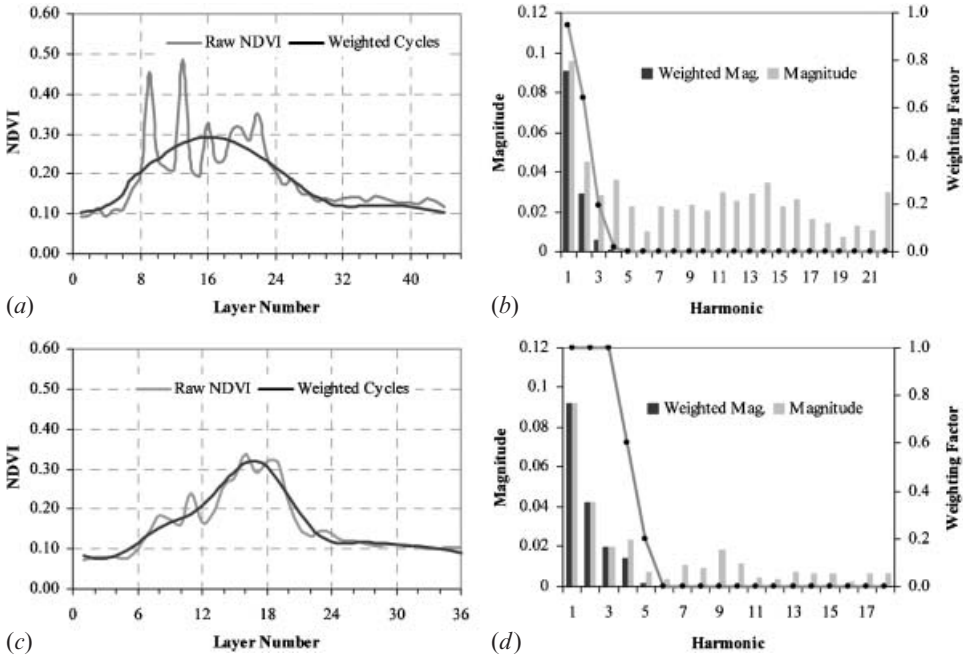

Figure 13. Original and Fourier-filtered NDVI cycle from MODIS data (*a*) and from SPOT VEGETATION data (*b*). Filtering applied to the harmonics and the weighted magnitudes used in the inverse Fourier calculation are shown in *b* (MODIS) and *d* (SPOT) (Geerken *et al.* 2005).

NDVI and 0.94 for SPOT NDVI (figure 14). To achieve a similar classification result from the SAVI time series we had to admit lower-correlating pixels with a minimum correlation value of 0.96 for MODIS and 0.92 for SPOT. The difference is not significant, but may be caused by temporal variable noise that is better smoothed by a ratio index such as the NDVI (Holben and Justice 1981) than by an index such as the SAVI that is a mixture of an orthogonal and a ratio index. In all the analyses, we further narrowed the classes by only admitting pixels with slope values ranging within defined limits, in this manner excluding unrealistically high and low vegetation coverages.

Out of a total of 114 sites identified in the field as 'extended' class, 106 were correctly identified in the MODIS analysis and 110 in SPOT. Of the 60 sites of the 'non-extended' class, 37 were incorrectly classified as extended with MODIS and 32 with SPOT. Of these field sites, 11 in MODIS and 16 in SPOT proved to be too small, 15 in MODIS and 11 in SPOT are located at the periphery suggesting spectral mixing effects, and 11 in MODIS and 5 in SPOT are incorrect.

While the classifications of MODIS data and of SPOT VEGETATION data show similar patterns in the densely grown areas, MODIS shows a larger area of scattered pixels extending to the west (figure 14(*b*)), not visible in the SPOT data. Many of these pixels are incorrectly identified and line up with cultivated fields. The reasons for this we believe are the noise in the MODIS reference cycle, especially the non-periodic noise such as the sporadic spikes (figure 13(*a*)), and the variable affection of the target cycles by similar noise features.

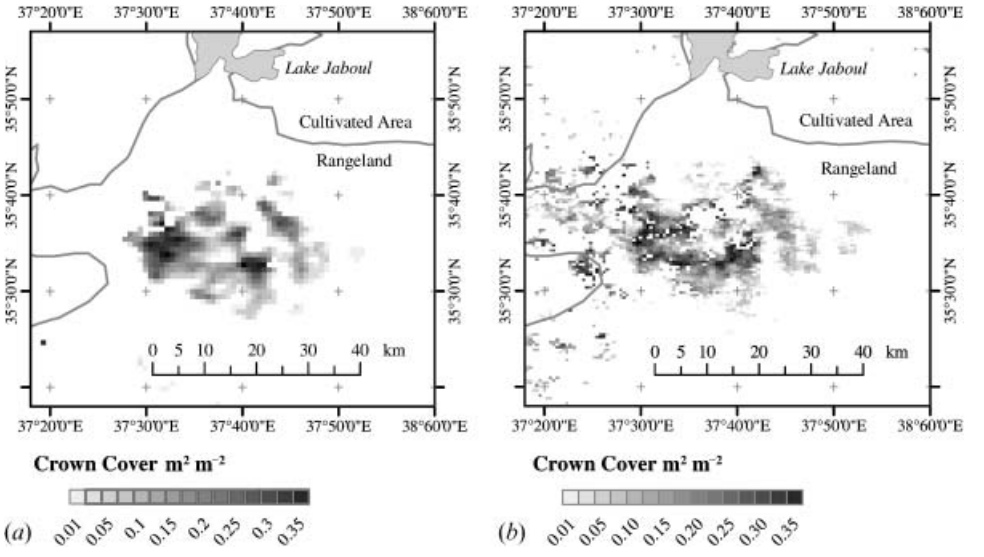

Figure 14. Pixels identified as 'vegetation cover with extended growing period' in SPOT NDVI time series (*a*) and in MODIS NDVI time series (*b*). Pixels were identified by correlating a NDVI reference cycle with the data set. The threshold applied to the correlation coefficient that identifies matching phenological cycles was 0.94 (SPOT) and 0.97 (MODIS). The corresponding slope values reflect variations in crown cover.

5.2 *Fractional shrub cover (VI–crown cover correlation)*

Technically, the slope values (resulting from the regression calculation) of the pixels identified as vegetation cover with an extended growing period are a relative measure of shrub crown cover to the reference site. Using field information from 21 sites, we tested how well the slope values derived from both NDVI and SAVI time series correlate with the actual shrub crown cover. The performance of slope/crown cover correlations was compared with correlations calculated between crown cover and single-date NDVI and SAVI layers (original and Fourier-filtered) acquired during the most diagnostic time period of the year (figure 4(*a*)). For the latter we chose MODIS and SPOT composite layers from 1 June. The correlation coefficient and the level of significance for each correlation are given in table 4. For MODIS and SPOT, the maximum correlation and the highest level of significance were found between crown cover and the slope values derived from the NDVI time series, with the results calculated from SPOT being a little higher (correlation coefficient 0.72, significance 0.999) than those calculated from MODIS (correlation coefficient 0.63, significance 0.995). The generally lower correlation coefficients and the lower significance levels of single-date layers are attributed to rangeland-typical low VI values and to small VI variations during the diagnostic dry season period. Correlations derived from SAVI time series were always lower than those of their NDVI analogue. The better performance of the NDVI is attributed to the poorer noise suppression by the SAVI. In contrast to our field measurements, the NDVI also performed better when correlating between coverage and a vegetation index of a single layer (here 1 June; see table 4). Again, we attribute this to pixel-specific noise, introduced by the 8-day compositing process. This is supported by the corresponding view angles of the 44 MODIS (36 SPOT) layers showing a very

Table 4. Correlation coefficients calculated between the coverage of species with an extended growing period (shrubs) and various vegetation indices.

	Sensor											
	MODIS						SPOT VEGETATION					
Coverage correlated with: Date:	NDVI 06/01	SAVI 06/01	NDVI ff 06/01	SAVI ff 06/01	Slope NDVI	Slope SAVI	NDVI 06/01	SAVI 06/01	NDVI ff 06/01	SAVI ff 06/01	Slope NDVI	Slope SAVI
Correlation Coefficient	0.61	0.51	0.54	0.52	**0.63**	0.49	0.45	0.29	0.48	0.35	**0.72**	0.56
Significance	0.995	0.975	0.99	0.99	**0.995**	0.975	0.975	0.8	0.975	0.9	**0.999**	0.99

Note: Correlation and significance of best performing approach for biomass assessment are indicated in bold values.
ff, Fourier-filtered.

heterogeneous pattern, not only temporally between layers but also spatially within one layer. The latter indicates that layers were composited of pixels acquired at different times, and probably under varying atmospheric conditions.

Shallow view angles also cause pixels to be stretched out in the view direction, leading to considerable deviations from their highest resolution in the nadir position. The average elongation of all pixels representing our sampling points and averaged over the entire hydrological year is 1038 m (MODIS) and 2634 m (SPOT). The maximum elongation measured is 2347 m (MODIS) and 4654 m (SPOT); the absolute minimum is 500 m (MODIS) and 1178 m (SPOT). Though a correlation coefficient of 0.63 and 0.72 is acceptable, we cannot rule out the possibility that high variability in viewing angles does have an impact on our correlation calculations that attempt to link field-measured vegetation coverage to some image-derived parameter. Some of our field locations actually may prove to be too small to fill pixels that were acquired under extreme viewing angles.

Stronger correlations and higher significance levels of a single-date MODIS NDVI or SAVI layer compared with SPOT are the result of the higher dynamic range (11-bit MODIS compared with 8-bit SPOT) triggering higher slope values in crown cover/VI correlations. Correlating NDVI or SAVI layers from other dates including the vegetation peak with crown cover produced very mixed results. Vegetation indices dating from the vegetation peak performed much better for SPOT but considerably poorer for MODIS. All correlations, except for the MODIS NDVI from 1 June, improved when using the corresponding Fourier-filtered vegetation index layers instead (table 4). The good performance of the slope values for describing crown cover we interpret as the result of successful noise suppression using Fourier-filtering, and to the fact it is an integrative parameter computed from the entire time series, not just a single-date value, which mitigates the impact of sporadic noise features.

In his study of range vegetation in Iraq, Thalen (1979) found strong linear correlations between current season's growth or aerial biomass and various crown attributes, including the longest diameter (D_1), the crown cover or the crown volume. He concluded that the plant height might be an important attribute for some species, but height did not correlate extremely well with the dwarf shrubs he studied. While the correlation between aerial biomass and crown cover for all studied dwarf shrubs is rather stable when measured at different times, the corresponding slopes vary between a minimum of 0.0438 in June to a maximum of 0.2567 in April. This variation in the biomass–crown cover relationship makes it difficult to calculate an accurate biomass at a certain time just from the crown cover and without making use of the empirical relationships that Thalen (1979) established. One has to assume that these relationships are submitted to temporal shifts depending on inter-annual climate variations, which will further complicate their use. For this reason, an accurate breakdown of the total green biomass (e.g. produced by shrubs with an extended growing period and green biomass produced by annual grasses) is not possible.

6. Conclusions

Distinct vegetation types can be identified based on phenological characteristics that manifest in their NDVI cycles. Temporal and spatial resolution of NDVI data from MODIS (MOD9A1) and SPOT VEGETATION are suitable to capture differences

in the growing cycles of studied vegetation types. A meaningful evaluation of phenolgies should focus on a description of the shape of NDVI cycles. Simple linear regression calculation proved to be useful to measure similarity (correlation coefficient) between two quasi-normally distributed NDVI cycles and, of particular importance for rangelands, to estimate vegetation coverage (slope).

Closely linked to the plants' phenology are functional characteristics, including palatability and certain hydro-meteorological properties, which are essential when describing ecosystem health, ecosystem processes or its resources. For a meaningful assessment and monitoring of rangelands, therefore, analyses using remotely sensed data should concentrate on proper approaches that help to describe NDVI cycles. A more complete study of plant phenologies and their NDVI cycles will be needed to fully understand the information contained in the shapes of NDVI cycles, what is influencing them, and which functional characteristics we can derive from them.

Varying functional characteristics of plants trigger differences in plant phenology, also influencing the plants' temporal-spectral characteristics. This causes some variation in correlation between the plants' green biomass and spectral reflectance. For a balanced biomass estimation of all our vegetation types, our analyses recommend a narrow banded (9 nm width) NDVI that uses bands 630 nm (505 nm) and 755 nm (755 nm). The individual assessment of biomass production for a distinct vegetation type in a mixed vegetation cover was not possible, because the trends in crown cover–biomass relationships are not constant over a growing season.

Acknowledgements

This study was carried out as part of the project 'Environmental Changes in South West Asia' (NAG5-9316) as well as 'The Water Cycle of the Tigris–Euphrates Watershed: Natural Processes and Human Impacts' (NNG05GB36G), both funded by NASA. We wish to thank NASA for its financial support and the people who facilitated this study through their support in the field and in the laboratory, particularly Zuhair Masri from the International Center of Agricultural Research in the Dry Areas (ICARDA). We are grateful to the anonymous referees for their useful comments on the manuscript.

References

Duncan, J., Stow, D., Franklin, J. and Hope, A., 1993, Assessing the relationship between spectral indexes and shrub cover in the Jordana Basin. *International Journal of Remote Sensing*, **14**, pp. 3395–3416.

Dunkerley, D., 2000, Hydrologic effects of dryland shrubs: defining the spatial extent of modified soil water uptake rates at an Australian desert site. *Journal of Arid Environments*, **45**, pp. 159–172.

El-Bana, M.I., Nijs, I. and Khedr, A.H.A., 2003, The importance of phytogenic mounds (nebkhas) for restoration of arid degraded rangelands in northern Sinai. *Restoration Ecology*, **11**, pp. 317–324.

Elvidge, C.D., 1990, Visible and near-infrared reflectance characteristics of dry plant materials. *International Journal of Remote Sensing*, **11**, pp. 1775–1795.

Elvidge, C.D. and Chen, Z., 1995, Comparison of broad-band and narrow-band red and near-infrared vegetation indices. *Remote Sensing of Environment*, **54**, pp. 38–48.

Evans, J. and Geerken, R., 2004, Discrimination between climate and human induced dryland degradation. *Journal of Arid Environments*, **57**, pp. 535–554.

FAO, 1990, Management of gypsiferous soils. *FAO Soils Bulletin 62* (Rome: FAO).

Geerken, R. and Ilaiwi, M., 2004, Assessment of rangeland degradation and development of a strategy for rehabilitation. *Remote Sensing of Environment*, **90**, pp. 490–504.

GEERKEN, R., ZAITCHIK, B. and EVANS, J.P., 2005, Classifying rangeland vegetation type and fractional cover of semi-arid and arid vegetation covers from NDVI time-series. *International Journal of Remote Sensing* (in press).

HUETE, A.R., JACKSON, R.D. and POST, D.F., 1985, Spectral response of plant canopy with different soil backgrounds. *Remote Sensing of Environment*, **17**, pp. 37–53.

HUETE, A.R. and JACKSON, R.D., 1987, Suitability of spectral indices for evaluating vegetation characteristics on arid rangelands. *Remote Sensing of Environment*, **23**, pp. 213–232.

HUETE, A.R., 1988, A soil-adjusted vegetation index (SAVI). *Remote Sensing of Environment*, **25**, pp. 295–309.

HOLBEN, B.N. and JUSTICE, C.O., 1981, An examination of spectral band ratioing to reduce the topographic effect on remotely sensed data. *International Journal of Remote Sensing*, **2**, pp. 115–133.

LEHOUÉROU, H.N., 1996, Climate change, drought and desertification. *Journal of Arid Environments*, **34**, pp. 133–185.

LEWIS, M., 2000, Discrimination of arid vegetation composition with high resolution CASI imagery. *Rangeland Journal*, **22**, pp. 141–167.

NORDBLOM, T.L., GODDCHILD, A.V., SHOMO, F. and GINTZBURGER, G., 1996, Dynamics of feed resources in mixed farming systems of North Africa, West and Central Asia. In *Regional International Workshop on Crop Residues in Sustainable Mixed Crops/ Livestock Farming Systems, ICRISAT*, Patancheru, India, 22–26 April 1996.

OKIN, G.S., ROBERTS, D.A., MURRAY, B. and OKIN, W.J., 2001, Practical limits on hyperspectral vegetation discrimination in arid and semiarid environments. *Remote Sensing of Environment*, **77**, pp. 212–225.

PETERS, A.J., EVE, M.D., HOLT, E.H. and WHITFORD, W.G., 1997, Analysis of desert plant community growth patterns with high temporal resolution satellite spectra. *Journal of Applied Ecology*, **34**, pp. 418–432.

PICKUP, G., BASTIN, G.N. and CHEWINGS, V.H., 1998, Identifying trends in land degradation in non-equilibrium rangelands. *Journal of Applied Ecology*, **35**, pp. 365–377.

QI, J., MORAN, M.S., CABOT, F. and DEDIEU, G., 1995a, Normalization of sun/view angle effects using spectral albedo-based vegetation indices. *Remote Sensing of Environment*, **52**, pp. 207–217.

QI, J., CABOT, F., MORAN, M.S. and DEDIEU, G., 1995b, Biophysical parameter estimations using multidirectional spectral measurements. *Remote Sensing of Environment*, **54**, pp. 71–83.

RAE, J., ARAB, G., NORDBLOM, T., JANI, K. and GINTZBURGER, G., 2001, Tribes, state, and technology adoption in arid land management, Syria. In *CGIAR Systemwide Program on Collective Action and Property Rights, CAPRi Working Paper No. 15* (Washington, DC: IFPRI).

RICHARDSON, A.J. and WIEGAND, C.L., 1977, Distinguishing vegetation from soil background information. *Photogrammetric Engineering and Remote Sensing*, **43**, pp. 1541–1552.

THALEN, P., 1979, Ecology and utilization of desert shrub rangelands in Iraq. PhD thesis, Rijksuniversiteit Groningen (The Hague: W. Junk).

TUCKER, C.J., DREGNE, H.E. and NEWCOMB, W.W., 1991, Expansion and contraction of the Sahara Desert from 1980 to 1990. *Science*, **253**, pp. 299–301.

UNEP, 1992, *World Atlas of Desertification* (London: Edward Arnold).

WEISS, E., MARSH, S.E. and PFIRMAN, E.S., 2001, Application of NOAA-AVHRR NDVI time-series data to assess changes in Saudi Arabia's rangelands. *International Journal of Remote Sensing*, **22**, pp. 1005–1027.